

# CFD AND FEA USED TO IMPROVE THE QUENCHING PROCESS

*Mathematical tools such as computational fluid dynamics (CFD) and finite element analysis (FEA) can be used in combination to improve the response of metal components to heat treatment processes that include quenching. The combination of CFD and FEA modeling techniques provides an efficient and effective method for the design of quenching processes and related fixtures.*

**Andrew Banka\***  
**Jeff Franklin**

Airflow Sciences Corp.  
Livonia, Mich.

**Zhichao Li\***

**B. Lynn Ferguson\*, FASM**  
Deformation Control Technology Inc.  
Cleveland, Ohio

**Michael Aronov\***

IQ Technologies Inc.  
Akron, Ohio

**Q**uenching of steel components is a fast transient thermal process where the part is heated above the austenitization temperature, and rapidly cooled by the quenching media. The most common quenching processes include immersion in a liquid, spraying the heated part with a liquid, and blowing a gas onto and around heated parts. Liquid quenching includes immersion into an oil, plain water, brine, water/polymer, or molten salt medium. For all quenching methods, the quenchant flow condition has a primary effect on the quenching results, including final microstructural phase distribution, hardness, residual stress, and part distortion. Knowledge and control of the quenchant flow is important for controlling the quenching process and for achieving the desired results. With computational fluid dynamics (CFD) technologies, the quenchant flow pattern during quenching can be calculated. In one published study, the oil velocity in a quench tank was predicted by static CFD analysis using FLUENT (Ansys Inc, Lebanon, N.H.; [www.fluent.com](http://www.fluent.com)) and the information was used to predict the cooling uniformity among parts in a quenching rack, as well as the local cooling differences within a single part<sup>[1]</sup>. The quenchant velocities from the CFD model were converted to heat transfer coefficients along the part surfaces and used as thermal boundary conditions in the DCT's DANTE heat treatment model to predict part distortion<sup>[2]</sup>.

Intensive quenching methods were developed more than 30 years ago by Nikolai Kobasko and others<sup>[3]</sup>. Intensive quenching uses plain water or water-salt solutions as the quench media, and it achieves extremely high cooling rates in the steel parts. Due to the high thermal gradient and rapid surface and near-surface formation of martensite early during the quenching process, intensive quenching can generate high compressive residual stresses in the part surface. High surface compressive residual stresses are desirable in many applications to improve the fatigue life of the heat treated

part. Studies have shown that intensive quenching can be applied to both carburized and non-carburized steel parts, which makes it an attractive quench hardening process for steel gears<sup>[4-6]</sup>.

During intensive quenching, high speed water flows along the surface of the part to extract heat quickly and uniformly. Film boiling must be avoided, and even nucleate boiling during quenching, where the heat transfer is typically high, is not desired. However, water flow at concave locations of the part may be stagnant, which will cause a much lower cooling rate than the average. Conversely, the cooling rate at outer corners and edges can be much higher than the average, which may cause cracking at these locations due to excessive thermal stresses. Fixtures for intensively quenching individual parts can be designed to direct the water flow more uniformly along the surface of the part to improve uniformity of cooling. In this study, CFD predictions of the water flow field and surface heat transfer rates along a gear are used to characterize and improve the performance of an intensive quench fixture. The quenchant temperature and heat transfer coefficients along the gear surfaces are then used as input to drive DANTE models to predict the metallurgical, stress, and distortion responses of the gear for the fixture design.

## CFD Modeling

The intensive quench fixture in this study was designed to emphasize cooling of the gear teeth, especially the root area between teeth. Water is directed radially inward into the root area (Fig. 1). The incoming water flows down the pipe, is diverted outward by an upper cone, and enters the gear chamber radially. A portion of the flow travels over the top surface of the gear and down through the bore, while the balance flows under the gear and out through the bottom tube.

The heat flux rate on the surface of the gear is expected to vary from location to location due to several factors, including: 1) variations in the velocity in the vicinity of the gear tooth; 2) the

\*Member of ASM International and member, ASM Heat Treating Society

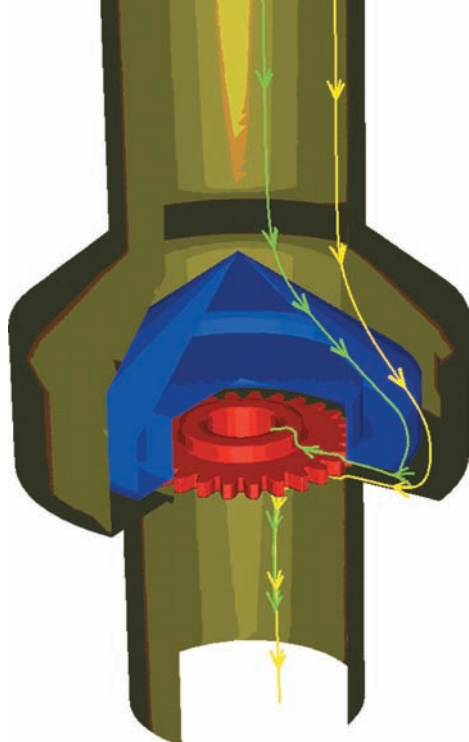


**Fig. 1 —** Cutaway view of the quench fixture showing the gear (red), upstream deflector (blue), and representative water path lines passing over and under the gear (green, yellow).

thickness of the velocity boundary layer; and 3) the thickness of the thermal boundary layer. Accurate prediction of these effects requires a CFD model with a high mesh density around the part, with sufficient number of near-surface grid points. While it is expected that the heat flux rates will vary greatly with time, it is not clear that these rates will vary in the same way at different surface locations. Due to the high heat flux rates and rapid temperature changes in-

herent in the intensive quenching process, the transients are expected to be brief.

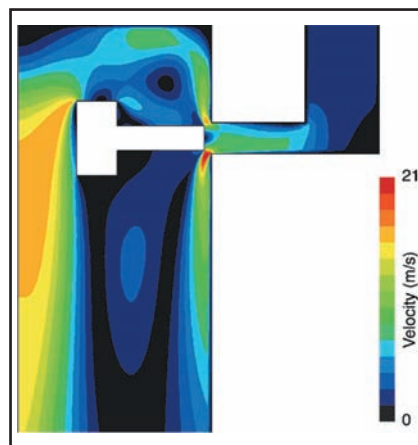
It seems that a full 3-D transient analysis is necessary to fully characterize the heat flux rates throughout the process, but such a simulation is currently impractical due to the computing resources needed. Instead, a method was developed wherein a 2-D transient model was used to characterize the variations in heat transfer due to location and time in the quench process, which is used to predict the 3-D transient heat flux rates.

CFD simulations discussed in this article assume that boiling phenomena are short-lived and have no major impact on the resulting material properties, which is reasonable for high-velocity intensive quenching processes.

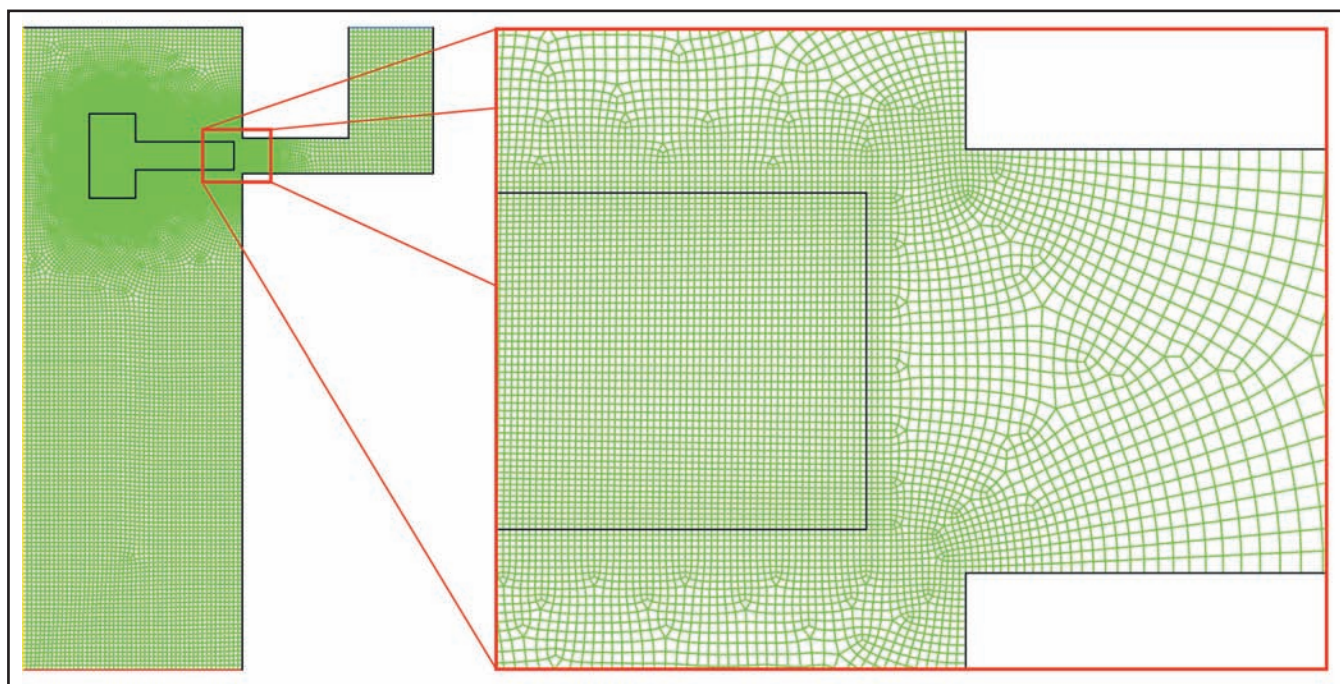
## 2-D Axisymmetric CFD Modeling

Figure 2 shows the domain and the computational grid used for the 2-D CFD model. The geometry of the 2-D solid used in this model is equivalent to a 3-D gear blank before the teeth are hobbled. More than 50,000 computational cells were used for this model, with about 22,000 cells within the gear blank solid. Figure 2 shows the cells adjacent to the gear were tightly spaced to capture flow gradients. The standard wall function model within FLUENT was used for all simulations. A total quench time of 10 seconds was simulated.

Figure 3 shows the magnitude of velocity at the beginning of the intensive



**Fig. 3 —** Total velocity plot of water flowing through quench fixture and around gear blank.



**Fig. 2 —** Domain and mesh for the 2-D CFD simulation.



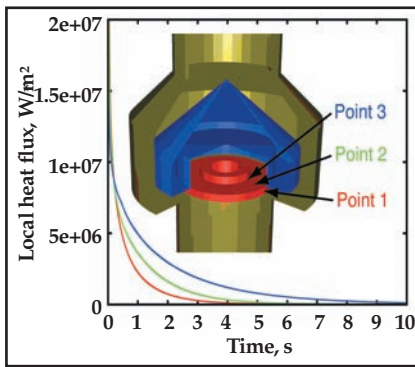


Fig. 4 — Time history of surface heat flux for three points on gear blank from 2-D transient simulation.

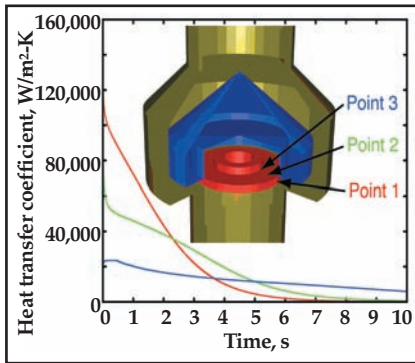


Fig. 5 — Time history of surface heat transfer coefficient for three points on gear blank from 2-D transient simulation.

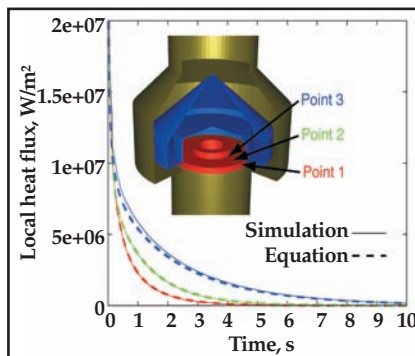


Fig. 6 — Comparison of simulated heat flux values and estimated values for 3 points on the 2-D gear blank model.

quench. High velocities are predicted at the outside corners of the gear blank. The large faces of the gear blank web are predicted to experience lower velocities that will result in lower heat flux rates. The tooth face of the gear blank is exposed to impinging flow, and is expected to have high heat transfer due to the water temperature and flow direction even though the local velocities are relatively low. This velocity pattern is predicted to remain largely unchanged throughout the duration of the quench cycle.

Figure 4 shows the time history of the heat flux at 3 points on the surface of the gear blank. These points highlight the behavior for regions with significantly different water flow conditions. While the initial heat flux rates differ by a factor of more than 4, all curves asymptotically approach zero at long times. Figure 5 shows the time history of the heat transfer coefficient at these three points. Again, the values vary widely both by location and by time. Thus, the assumption of a uniform heat transfer coefficient for the quenching process does not properly represent the quenching environment.

### Development of Correlation Function

As noted above, it is possible but not currently practical to perform a full 3-D transient simulation of complex geometries to define the heat transfer rates during quenching. Nevertheless, the 2-D model presented above shows that the heat flux rates and heat transfer coefficients vary considerably with time and location. The challenge is to extract sufficient information from one or two steady-state CFD simulations to characterize the heat transfer rates over the entire quench cycle. Such a characterization is expected to provide significantly improved accuracy over current methods, which typically assume a constant heat transfer coefficient.

Equation 1 was found to provide an accurate representation of the overall trends for the heat transfer rates on the 2D gear blank. It attempts to blend steady-state simulation results obtained from hot and cold conditions in a way that largely duplicates the actual transient behavior.

$$q = \left\{ h^o \frac{T_w - T_r}{T_w^o - T_r} + h^f \frac{T_w^o - T_w}{T_w^o - T_r} \right\} \left\{ T_w - \left( T_o \frac{T_w - T_r}{T_w^o - T_r} + T_r \frac{T_w^o - T_w}{T_w^o - T_r} \right) \right\} \text{eq. [1]}$$

where  $h^o$  is the initial local heat transfer coefficient,  $h^f$  is the final local heat transfer coefficient (when the part is

fully cooled), is the initial temperature of the part  $T_r$  is the reference fluid temperature (inlet fluid temperature),  $T_o$  is the initial near surface characterization temperature, and  $T_w$  is the current wall temperature. Note that the local heat transfer coefficients used in Eq 1 differ from those presented in Fig. 5, where the temperature differential is between the surface and the fluid inlet temperature, while the temperature differential for the local heat transfer coefficient is between the surface and the near surface fluid temperature.

The first term in Eq 1 provides a blending from the initial local heat transfer coefficient to the final value, while the second term provides the temperature differential, including a blending of the near surface liquid temperature from the initial to final values. Three variables in this equation are obtained from the CFD simulations;  $h^o$  and  $T_o$  are obtained from a steady-state simulation with the part surface held at its initial temperature, while  $h^f$  is obtained from a steady-state simulation with the part surface at the water inlet temperature. These values are independently found for each surface location on the gear, and later applied to the DANTE model.

Figure 6 shows the correlation between the simulated heat flux values from the transient simulation compared to the values predicted by the equation. Very good correlation is seen for Points 1 and 2. The correlation for Point 3 is not as good, most likely due to poor water flow in this area.

### Steady-State 3-D CFD Modeling

The grid used for the steady-state 3-D CFD modeling is shown in Fig. 7. The inherent symmetry of the geometry was used to reduce the domain to a half gear tooth. A total of 1,721,070 computational cells were used in the model. The gear solid was not included in the model. Instead, the gear surface temperature was specified on the boundary of the fluid domain. The model was run for both the hot part surface and the ambient part surface in order to determine the  $h^o$ ,  $h^f$ , and  $T_o$  values in equation 1.

The heat transfer coefficients are displayed in Figs. 8 and 9. The bottom side of the gear is displayed in these figures, as those surfaces show a greater variation than the top side. As suggested in Fig. 3, more of the fluid passes under the gear than over it, leading to the highest heat transfer rates on the lower corner of the gear

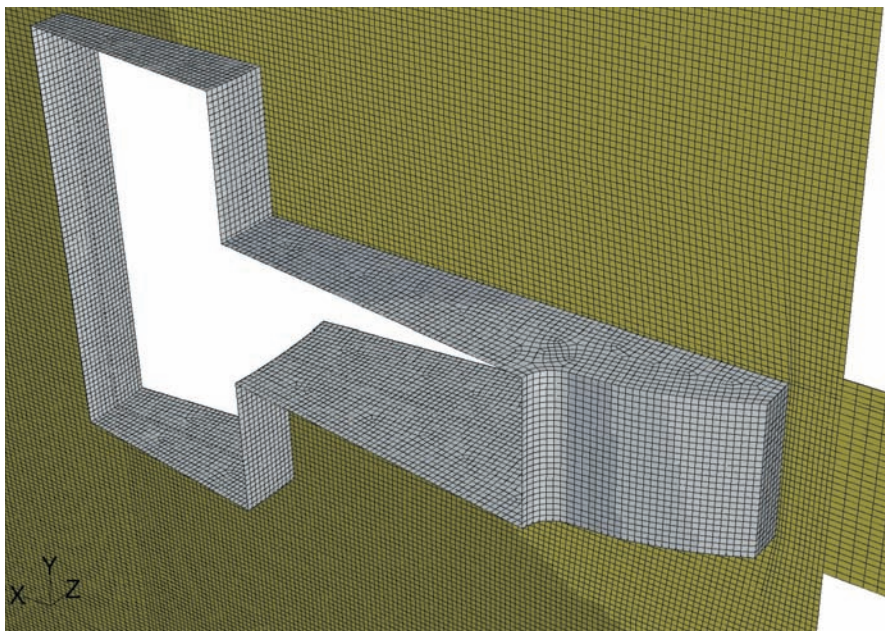


Fig. 7 — Computational domain and grid used for 3-D gear model.

tooth. This is seen for both the initial and final local heat transfer coefficients.

### Heat Treatment Model

In this study, the CFD model and the heat treatment model used different meshes. However, the element sizes in the heat treatment model were designed so that the heat transfer boundary conditions reported from CFD results could be effectively applied. A single tooth finite element model with 5,979 nodes and 4,820 hexahedral elements was created to predict the gear response during the intensive quenching process (Fig. 10).

The bore diameter of the gear is 30 mm, and the tip diameter of the 28-tooth gear is 95.25 mm. The heat treatment process included furnace heating, carburization, and intensive quenching. Results for subsequent cryogenic treatment and tempering are not included in this article, but they have been reported elsewhere<sup>[5]</sup>. During carburization, only the gear tooth surface was carburized, as all the other surfaces including the tooth tip were copper plated. Fine elements were used in the tooth surface to catch the carbon gradient.

Cyclic symmetric boundary conditions were used for both the thermal and stress heat treatment models. This assumption is based on the response of all the 28 gear teeth being same. This type of model cannot predict ovality and “potato-chip” distortion. Radial and axial distortion of the gear tooth are reported.

### Modeling the Carburization Process

The gear is made of Pyrowear 53 steel (Carpenter Technology, Reading, Pa.; www.carttech.com), which has a base carbon content of 0.1%. The gear is gas carburized at a temperature of 927°C for 8 h; carburizing potential is 0.8%. The predicted carbon contour plot after the carburization process is shown in Fig. 11(a). Line EF is located in the gear root around the fillet, as shown in Fig. 11(a). The predicted carbon distribution in terms of depth from the gear surface along line EF is shown in Fig. 11(b). The effective case depth is about 0.6 mm and the surface carbon is 0.8%.

### Analysis of Heat Treatment Modeling Results

The correlated heat flux based on Eq 1 was used as the thermal boundary condition to drive the DANTE heat treatment model. The heat transfer coefficients and the local ambient temperatures are dependent on both the surface of the part and quenching time.

Two lines of nodes, shown as line AB and line CD in Fig. 12, were selected to investigate

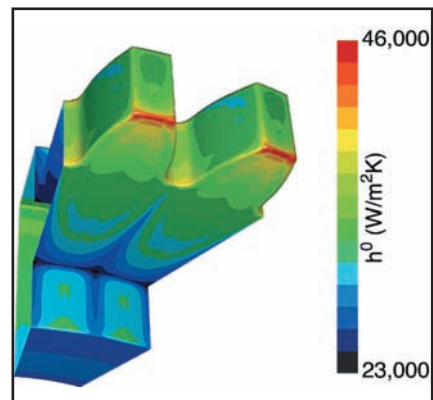


Fig. 8 — Initial local heat transfer coefficient values on the surface of the gear.

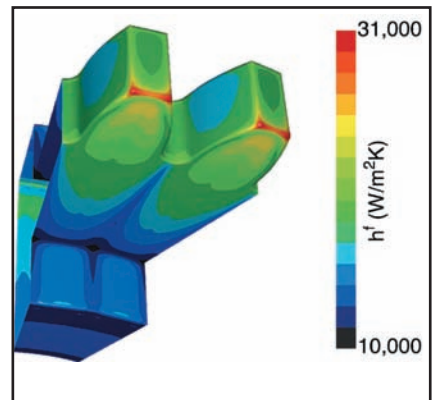


Fig. 9 — Final local heat transfer coefficients on the surface of the gear.

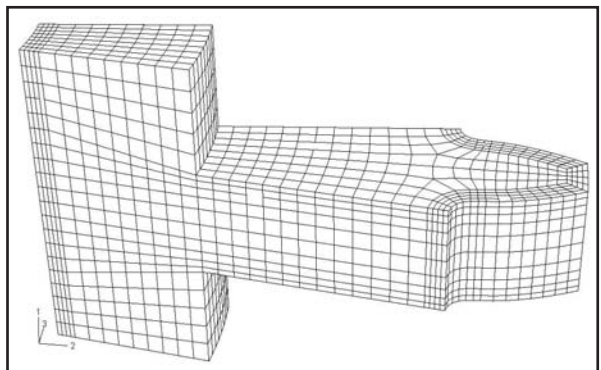


Fig. 10 — Finite element mesh used for the DANTE heat treatment model.

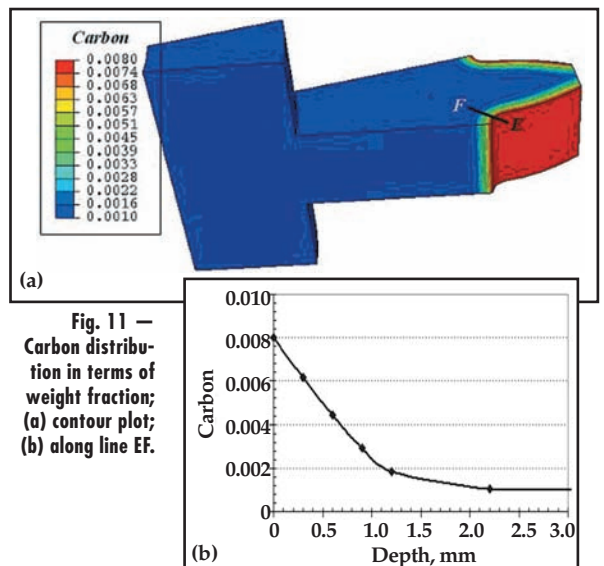


Fig. 11 — Carbon distribution in terms of weight fraction; (a) contour plot; (b) along line EF.



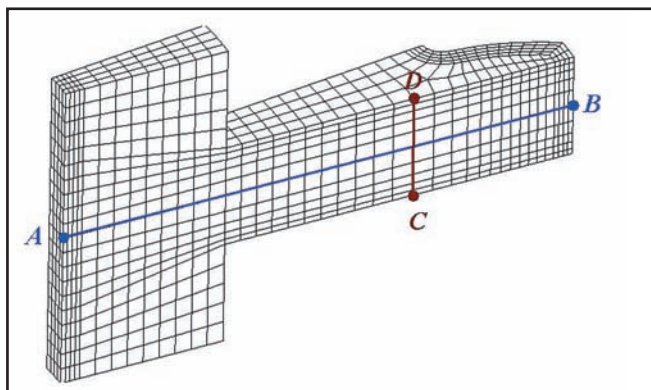


Fig. 12 — Lines AB and CD selected for heat treatment result analysis.

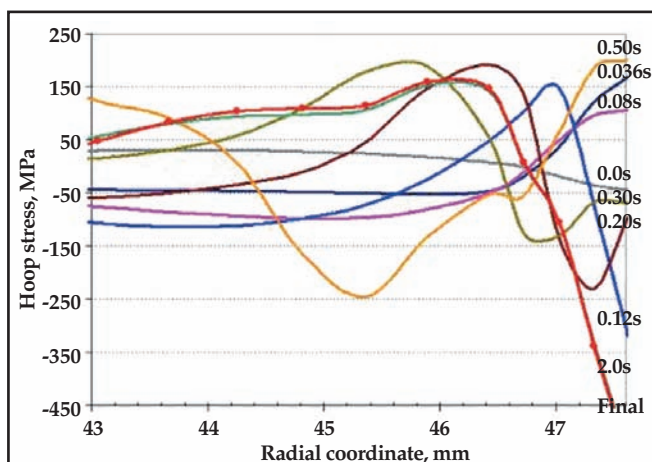
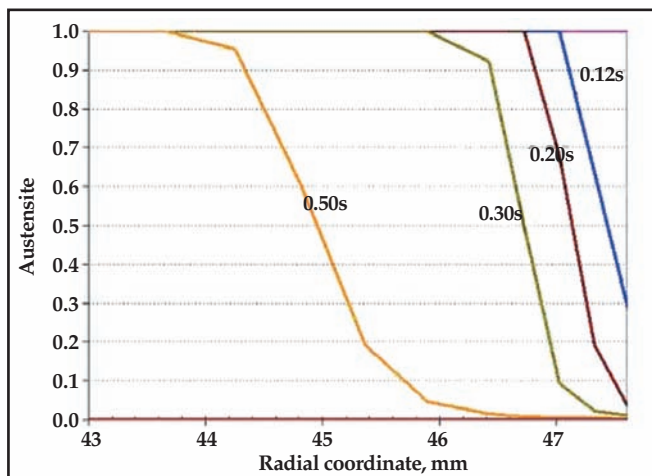
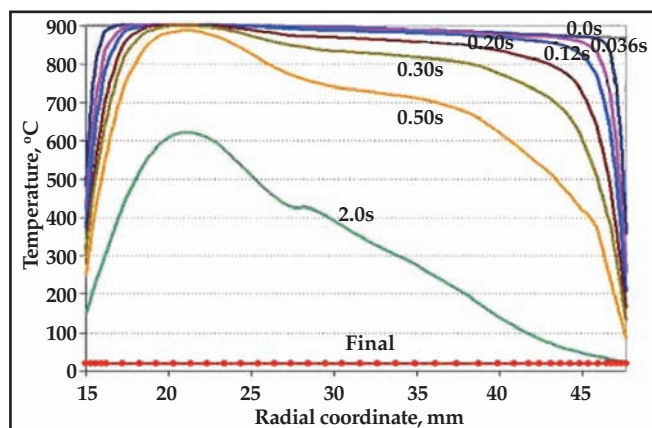


Fig. 13 — Temperature and phase transformation histories along line AB from DANTE simulation Rresults; (a) temperature history; (b) phase transformation history; (c) internal stress evolution.

the effects of temperature and phase transformations on the evolution of internal stress and distortion. Figure 12 shows half of the gear tooth cut through plane ACBD. Line AB is located at the half gear height. Both lines AB and CD are located on the half symmetry plane of the single gear tooth.

Pyrowear 53 has high hardenability due to its high alloy content. During the intensive quenching process, the only phase formed from austenite is martensite, and the sum of the volume fractions of austenite and martensite equals one. For reference, the martensite start temperature ( $M_s$ ) for the base carbon level of 0.1% is  $\sim 440^\circ\text{C}$  and the  $M_s$  of the 0.8% C surface is  $\sim 140^\circ\text{C}$ .

The gear was austenitized at  $927^\circ\text{C}$  in a salt pot, and there was a 10-s air transfer time to the quench unit. In Fig. 13, the radial coordinates of the line AB shown in Fig. 12 form the x axis. The centerline of the gear has a radial coordinate of zero. Figure 13(a) shows the temperature distributions along line AB at different quench times. The temperature distribution at the end of the air transfer stage is shown as the line marked with 0.0 s in Fig. 13(a). The temperature at point A (the bore of the gear) has dropped to about  $900^\circ\text{C}$ , and the temperature at point B (the tip of the gear) has dropped to  $870^\circ\text{C}$ , so the temperature at the tooth tip is  $30^\circ\text{C}$  lower than the temperature of the bore at the start of intensive quenching.

During the early stages of intensive quenching, a steep thermal gradient at the part surface is quickly established due to the high rate of heat extraction. Interpretation of model results requires that temperature, metallurgical phase and stress results be examined in concert because of the gear tooth shape, differences in local carbon contents, and, thus, differences in local martensite formation, and the steep temperature gradients.

Figure 13(b) shows the austenite distribution along line AB at indicated quenching times. The martensitic transformation starts at the tip surface at a time between 0.08 and 0.12 s. The transformation in the low carbon tip surface is nearly complete after about 0.5 s quenching. Compared with traditional oil quenching, the cooling rate for intensive quenching is much higher.

During quenching of steel parts, the thermal gradient and phase transformations are the two main contributions to internal stress. Figure 13(c) shows the hoop stress along line AB at indicated quenching times. The stress in the gear after austenization is sufficiently low that it can be assumed to be stress free. The carburization process introduces a slight compressive stress in the carburized gear surface. During the 10-s transfer time to the quench unit, the temperatures of the gear tooth surface (carburized) and gear tip surface drop. The temperature decrease at the gear tip surface causes local thermal contraction, which introduces tensile stress component at point B. At the same time, the temperature decrease at the carburized gear tooth surface imposes a compressive stress at point B due to a geometry effect. This combined effect generates a compressive hoop stress of 45 MPa at point B, as shown by 0.0 s line in Fig. 13 (c).

At 0.036 s during intensive quenching, a tensile hoop stress of 170 MPa is predicted at point B purely due to greater thermal contraction of the cooler surface compared with the hotter subsurface. No phase transformation has occurred at this time. As the surface continues to rapidly cool, higher surface tension leads to local plastic deformation of the surface in the early quenching stage due to the high thermal gradient. This is one key to the final residual stress generated in this carburized part. At 0.08 s, the cooling rate at the

subsurface exceeds the cooling rate at the surface since the surface is nearly at the water temperature. The surface tensile hoop stress drops from 170 to 105 MPa after 0.08 s of quenching. Figure 13(b) shows the martensitic transformation starts between 0.08 and 0.12 s at point B, during which time the phase transformation rate on the tooth tip surface is higher than that of the subsurface. Due to the material expansion caused by martensitic transformation, point B on the tip surface has a 320 MPa hoop stress in compression at the end of 0.12 s quenching. To balance the surface compressive stress, a tensile stress peak of 150 MPa is observed at the depth of about 0.5 mm from the tip surface, which is also the location of the transformation interface, as shown by the 0.12 s line in Fig. 13(b) and (c). Note that line AB does not traverse through the carburized case, so carbon content is constant at the baseline level along this line. At this time, no martensite has begun to form in the carburized case.

With continued quenching, the phase transformation interface moves inward from the tip surface. Between 0.12 and 0.2 s, the phase transformation rate in the subsurface exceeds the transformation rate on the surface. As shown by the 0.2 s line in Fig. 13(c), the tensile stress peak also moves inward. A compressive stress peak is observed at the shallow depth from the tip surface; this is the location which has the highest martensite formation rate. From 0.2 to 0.3 s during intensive quenching, both the tensile and compressive stress peaks move inward from the tip, and the level of tip surface compression is reduced. At 0.5 s, the highest transformation rate occurs at the depth of 2.2 mm from the tip surface, as shown by the 0.5 s line in Fig. 13(b). The compressive stress peak is about 150 MPa, as shown in Fig. 13(c). The depth of the tensile stress peak at 0.5 s is about 6.0 mm from the tip surface, and the hoop stress value is 200 MPa in tension. Due to the combined effect of the thermal gradient and martensite phase formation, the hoop stress at point B (the gear tip surface) is about 200 MPa in tension after 0.5 s of quenching.

The intensive quench is essentially complete in about 2.0 s for this specific gear and gear steel. At the end of quenching, a compressive hoop stress of 550 MPa is predicted at point B (gear tip surface). Finite element analysis shows that both the thermal gradient and steel phase transformations are very important to the stress evolution during quenching. Plastic deformation of austenite under tension during quenching is also key to the final residual stress distribution.

The main purpose of applying CFD analysis results to the finite element model of the intensive quenching process is to accurately characterize the nonuniform thermal boundary conditions. Knowledge of the water flow pattern, the local velocity, and the quenchant ambient temperature along the gear surface is required for assigning meaningful heat transfer coefficients along the surface of the gear during the heat treatment analysis. Without CFD results, the assumed heat transfer boundary conditions have been constant and uniform conditions. Because the gear is symmetric to the plane ABCD and normal to the gear axis, for these assumed conditions, line AB always remains straight and parallel to the  $x$ -axis during the FEA analysis. With these assumed uniform thermal boundary condition on the gear, FEA analysis cannot predict warping distortion, which is shown in Fig. 14(c) by the line with hollow round marks. The ability to predict nonuniform heat transfer conditions due to nonuniform quenchant flow is an important aspect of CFD analysis. Nodes on line CD in Fig. 12 were selected to investigate how

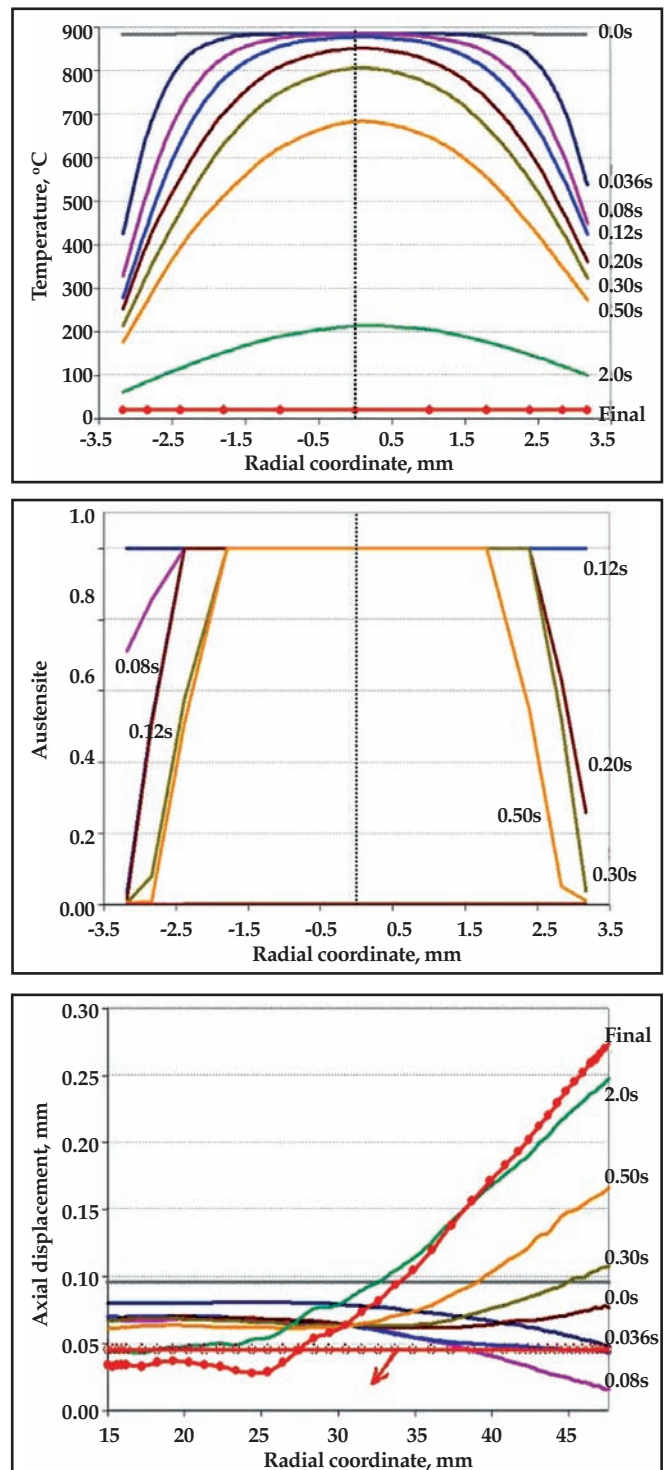


Fig. 14 — Generation of warping distortion; (a) temperature history along line CD; (b) phase transformation history along line CD; (c) displacement history along line AB.



Table 1 — Relationship of temperature difference and bow distortion

Quenching time, s	0.036	0.08	0.12	0.2	0.3	0.5	2.0	Final
$\Delta T$ , °C	110	121	147	109	108	97	39	0.0
Bowing, mm	-0.032	-0.051	-0.027	0.007	0.041	0.105	0.203	0.24

potential warping distortion is generated during intensive quenching. CFD analysis shows that the top and bottom surfaces of the gear hub cool differently during quenching. In Figure 14(a) and (b), the  $x$ -axis matches the nodal positions of line CD in Fig. 12 with point C locating on the left side of the  $x$ -axis and D to the right. Point  $X = 0$  is located at the midpoint of the line CD. In Table 1,  $\Delta T$  is the temperature difference between point C and point D at different quenching times. Warping distortion of the gear is defined as the difference of axial displacements at point A and point B at difference quenching times.

There is no phase transformation occurring along line CD before 0.036 s of intensive quenching, so the thermal gradient is the only cause of warping at this stage. At 0.036 s of quenching, the temperature at point C is about 425°C, and the temperature at point D is about 535°C. Greater thermal contraction at point C leads to 0.032 mm downward warping. At 0.08 s, the temperature difference between points C and D increases, and only a small amount of phase transformation occurs on the bottom hub surface. As a result, the warping distortion increases to 0.051 mm downward. At 0.12 s, the temperature difference between points C and D has increased to 147°C. The increased temperature difference increases the

warping distortion in the downward direction. However, the temperature on the bottom of the hub (point C) is well below the martensitic transformation starting temperature.

Martensitic phase transformation in the bottom surface causes material volume expansion, which compensates the downward warping due to temperature difference alone. As shown by the 0.12 s line in Fig. 14(c), the direction of warping starts to reverse. With longer time in quenching, the temperature difference between top surface and bottom surface decreases, and both top and bottom surfaces transform to martensite. The final warping distortion is about 0.24 mm in an upward direction.

## Conclusion

The results presented in this paper show that the quenchant flow field can have a significant effect on austenite decomposition, internal stress state, and distortion of the finished part. The combination of FLUENT CFD and DANTE heat treatment models can be effectively used in future studies to develop quench fixtures and processes that have improved uniformity of heat transfer, more desirable residual stress levels, and reduced distortion.

HTP

**Acknowledgement:** Research was sponsored by the U.S. Army Benet Laboratories and accomplished under Cooperative Agreement Number W15QKN-06-R-0501 between the Edison Materials Technology Center, Dayton, Ohio, and the U.S. Army.

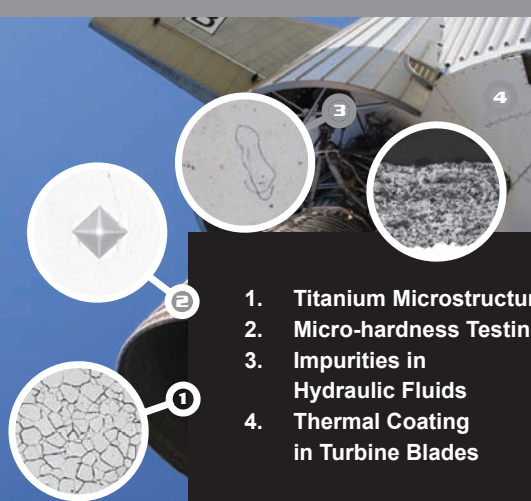
**For more information:** Dr. B. Lynn Ferguson, FASM, Deformation Control Technology Inc. 7261 Engle Rd., Suite 105, Cleveland, OH 44130; tel: 440-234-8477; e-mail: lynn.ferguson@deformationcontrol.com; Web site: www.deformationcontrol.com.

## References

1. D.S. MacKenzie, A. Kumar, and H. Metwally, "Optimizing Agitation and Quench Uniformity using CFD", Proceedings of the 23rd ASM Heat Treating Society Conference, 271-278, 2005.
2. D.S. MacKenzie, Z. Li, B. L. Ferguson, "Effect of Quenchant Flow on the Distortion of Carburized Automotive Pinion Gears", 5th International Conference on Heat Treatment: Quenching and Control of Distortion, 119-129, 2007.
3. N.I. Kobasko and N.I. Prokhorenko, "Quenching Cooling Rate Effect on Crack Formation of 45 Steel," Metallovedenie i Termicheskaya Obrabotka Metallov (in Russian), 53-54, 2(1964)
4. M.A. Aronov, N.I. Kobasko, J.A. Powell, J.F. Wallace, and D. Schwam, "Practical Application of the Intensive Quenching Technology for Steel Parts," *Industrial Heating*, 59-63, April 1999.
5. B.L. Ferguson, A. Freborg, and Z. Li, "Residual Stress and Heat Treatment- Process Design for Bending Fatigue Strength Improvement of Carburized Aerospace Gears", 5th International Conference on Heat Treatment: Quenching and Control of Distortion, 95-104, 2007.
6. C. Hubbard, F. Tang, "Effect of Intensive Quenching on Residual Stress", Proceeding of the 23rd ASM Heat Treating Society Conference, 338-342, 2005.

**CLEMEX** intelligent microscopy

**Quantitative  
Image Analysis  
in Aerospace**



1. Titanium Microstructure
2. Micro-hardness Testing
3. Impurities in Hydraulic Fluids
4. Thermal Coating in Turbine Blades

1.888.651.6573 • www.clemex.com